Vol. 43, 2/2005 ISSN: 1085–9195

Cell Biochemistry and Biophysics

Editor-in-Chief: **Edward J. Massaro**

Featured in this issue:

HUMANA PRESS

1085-9195/05/43:253–273/$30.00

ORIGINAL ARTICLE

Molecular Dynamics Simulation of a High-Affinity Antibody–Protein Complex

The Binding Site is a Mosaic of Locally Flexible and Preorganized Rigid Regions

Neeti Sinha[1,*] and Sandra J. Smith-Gill[2]

[1]106 Mudd Hall, Johns Hopkins University, 3400 N. Charles Street, Baltimore, MD 21218; [2]Structural Biophysics Laboratory, Center for Cancer Research, Building 538, National Cancer Institute at Frederick, National Institutes of Health, Frederick, MD 21702

Abstract

One nanosecond molecular dynamic (MD) simulation of anti-hen egg white lysozyme (HEL) antibody HyHEL63 (HH63) complexed with HEL reveals rigid and flexible regions of the HH63 binding site. Fifty conformations, extracted from the MD trajectory at regular time intervals were superimposed on HH63-HEL X-ray crystal structure, and the root mean squared deviations (RMSDs) and deviations in C_α atom positions between the X-ray structure and the MD conformer were measured. Residue positions showing the large deviations in both light chain and heavy chain of the antibody were same in all the MD conformers. The residue positions showing smallest deviations were same for all the conformers in the case of light chain, whereas relatively variable in the heavy chain. Positions of large and small deviations fell in the complementarity determining regions (CDRs), for both heavy and light chains. The larger deviations were in CDR-2 of light and CDR-1 of heavy chain. Smaller deviations were in CDR-3 of light and CDR-2 and CDR-3 of heavy chains. The large and small deviating regions highlight flexible and rigid regions of HH63 binding site and suggest a mosaic binding mechanism, including both "induced fit" and preconfigured "lock-and-key" type of binding. Combined "induced fit" and "lock-and-key" binding would be a better definition for the formation of large complexes, which bury larger surface area on binding, as in the case of antibody–HEL complex. We further show that flexible regions, comprising mostly charged and polar residues, form intermolecular interactions with HEL, whereas rigid regions do not. Electrostatic complementarity between HH63 and HEL also imply optimized binding affinity. Flexible and rigid regions of a high-affinity antibody are selected during the affinity maturation of the antibody and have specific functional significance. The functional importance of local inherently flexible regions is to establish intermolecular contacts or they play a key role in molecular recognition, whereas local rigid regions provide the structural framework.

Index Entries: Protein–protein interactions; flexibility; binding affinity; structure–function relationship.

*Author to whom all correspondence and reprint requests should be addressed. E-mail: nsinha1@jhu.edu.

INTRODUCTION

Understanding the fundamentals of protein binding and molecular recognition has been one of the challenges for present research, evidenced by myriad research articles covering these topics. Antibody–antigen complexes have been a unique archetype for both experimental and theoretical research to understand the basics of protein binding and protein–protein interactions *(1–10)*. Structural studies on these complexes highlight roles of different factors, such as electrostatics and entropy in binding *(8,11–14)*. Such factors, stemming from sequence details, determine the required flexibility *(15)* or rigidity with which protein–protein binding occurs.

Protein flexibility is important for function *(1,16–22)*. Protein molecules contain inherent flexible and rigid regions *(10,16,22)*. Protein active and binding sites are reported to contain flexible and rigid regions *(16,23,24)*. The important role of flexibility in antigen recognition by antibody has been noted *(25)*. Study of several conformations around the native state can potentially provide us with intricate and thorough details of protein dynamics in solution. Although there is evidence suggesting a general relationship of binding specificity and affinity to conformational flexibility (*26,27*), studies linking flexible and rigid regions to molecular recognition have not been undertaken. Such information would enhance drug design and our understanding toward basics of protein–protein interactions *(20–22)*.

The mechanism of protein ligand binding may be different than protein–protein binding because of significant difference in the amount of buried surface areas on associations. Comparisons of the structures between complexed and uncomplexed states have shown that antibody–antigen binding can be of "lock-and-key" *(28)* or of "induced fit" type *(29)*. Affinity maturation of hapten-binding antibodies appear to evolve from lower specificity, mediated by induced fit to higher specificity and reduced plasticity with a more "pre-configured" binding site *(28)*. It is intuitive that the antibody–protein complexes that bury larger surface area on binding, as compared with antibody–ligand complexes, will have flexible and rigid regions at different locations of their binding sites. This would mean that overall binding in large complexes would be partly induced-fit and partly lock-and-key type.

HyHEL63 (HH63) is a monoclonal antibody of high affinity toward hen egg white lysozyme (HEL) (K_A-3.5×10^8) *(13)*. Its epitope consists of about 15 residues at three different sequential locations, forming a contiguous patch at HEL molecule *(13)*. The complex buries a large surface area of 1901 $Å^2$ on binding. Twenty-four hydrogen bonds and extensive Van der Waals interactions connect HH63 with HEL. There are 11 water molecules present at the interface of HH63–HEL complex, linking HH63 to HEL via hydrogen bonds. It has an intermolecular salt bridge, $Asp32_H$-$Lys97_Y$, which involves complementarity determining region (CDR)-1 of the heavy chain and the most important "hot spot" epitope residue *(13,26,30)*. (Residue position is followed by chain identification in subscript through out the text: light chain [L]; heavy chain [H]; lysozyme [Y].) This salt bridge is proposed to significantly stabilize HyHEL63–HEL complex *(30)*. Superpositioning the bound form of HH63 on three forms of free HH63, crystallized in different space groups, respectively, showed that CDR-H2 and CDR-H3 deviate to relatively larger extents as compared with other CDRs *(13)*.

The present study was undertaken to (1) ascertain flexible and rigid regions of the antibody binding site; (2) understand the role of local flexibility/rigidity in antibody–protein binding and in molecular recognition in general; (3) determine whether or not lock and key mixed with induced-fit type of mechanism largely holds in the formation of this large protein–protein complexes; and (4) investigate the selection of charged and polar residues in flexible and rigid regions and to understand the functional significance of such selection. Fifty conformers, extracted at regular time intervals from the molecular dynamic (MD) trajectory,

were superimposed on the X-ray crystal structure of HH63–HEL and inspected for root mean squared deviations (RMSDs) and maximum and minimum c_α deviations. As expected, the RMSDs were small. The regions showing the highest and lowest deviations were same in all the conformers for the light chain. The heavy chain also showed the highest deviations at the same locations in all the conformers, whereas the region of lowest deviations were relatively variable, but confined to CDR-2 and CDR-3. The regions of large deviations and small deviations were located in different CDRs in both light and heavy chains. The CDRs showing flexible behavior throughout the MD simulation form relatively more intermolecular interactions with HEL via hydrogen bonds and salt bridges. In addition, we studied 100 conformations for intermolecular associations. The observations showed that highly deviating flexible residues were polar or charged and participated in intermolecular associations with HEL. This is consistent with an earlier study showing that flexible regions had larger charged and polar residues, and these residues participate in intermolecular interactions *(31)*. Rigid regions of the antibody do not form any direct contact with antigen and stay relatively away from the binding site as seen in the X-ray structure and in 100 MD conformers. The regions of intermediate flexibilities are in coils away from the binding site. These semiflexible coils may act as hinges for hinge-bending type movements *(17)* for conformational changes during binding.

Our calculations have shown significant electrostatic complementarity between HH63 and HEL—to a much larger extent than between HH10, belonging to the same family of antibodies, and HEL (1). High electrostatic complementation between and HH63 and HEL document the optimized HH63–HEL binding via inherent flexible and rigid regions acquired during the affinity maturation of this monoclonal antibody.

Previous studies have shown flexible and rigid areas at the antibody binding site based on the comparison between crystal structure in unbound and bound states. Here, based on explicit calculations, we show for the first time the presence of inherent flexible and rigid regions and the possible roles of these regions in binding. We conclude that the binding region of affinity matured antibodies consist of preselected locally flexible and rigid regions: flexible regions undergo induced-fit binding and function in molecular recognition or intermolecular associations, whereas rigid regions exhibit preconfigured conformation, providing structural framework.

MATERIALS AND METHODS

Molecular Dynamics Simulation

Molecular dynamics simulations were performed at constant temperature and volume in NVT canonical ensemble using velocity scaling method for temperature control and in the cubic periodic boundary conditions using C-DISCOVER at the INSIGHT-II interface. The initial velocities for all atoms were taken from Maxwellian distribution at the temperature of 298.0 K, employing the Verlet algorithms with a time step of 1 fs. The distance-dependent dielectric was employed, with the protein dielectric value of 4.0. Group-based cutoffs at 9.50 Å was used for the treatment of nonbonded interactions. The system consisted of variable domains, lysozyme, and water molecules in the crystal structure and another 7286 water molecules, making a total of 27,105 atoms per unit cell. All the atoms in the system were considered explicitly, and the interactions were computed using CFF91 force field *(32)*. The system was subjected for equilibration for 10 ps, before collecting data. One-nanosecond molecular dynamics was performed in five steps of 200 ps simulation each. The initial velocities for all atoms were taken from Maxwellian distribution at the temperature of 298.0 K, employing the Verlet algorithms with a time step of 1 fs. The dynamics, after each 200-ps step, was continued using the restart file, which contains all the internal coordinates and potential functions of the last conformation. The

current velocity was used with the restart file while continuing the MD. Total energy, potential energy, kinetic energy, and temperature showed steady behavior over the production run, suggesting that the sound equilibration was attained during the data collection stages. Snapshots from the trajectory were saved every 2 ps. Only 50 conformations at regular time interval (every 20 ps) were analyzed for the present study.

Superimposition of MD Conformers on the X-Ray Crystal Structure

The coordinates of HH63–HEL complex was extracted from the protein data bank (PDB) *(33)*. Each of the extracted MD conformers was superimposed on the X-ray crystal structure, and the RMSD and distances between corresponding C_α pairs between the two were calculated.

Assignment of Flexible and Rigid Regions

The flexible and the rigid regions of HH63 were assigned as described by Sinha and Nussinov *(16)*. Color assignment for the flexible and rigid regions were based on the mean of the C_α deviations of all MD conformers, against the wild-type. These were plotted. Two cutoffs were selected to illustrate the extent of the deviations. The region above the second cutoff was considered flexible and is shown in blue. The area below the first cutoff is considered to be rigid and is shown in red. The region between the two cutoffs is of intermediate flexibility and shown in green. The color assignments were using the method of Sinha and Nussinov *(16)*, described in Materials and Methods. The cutoffs for the blue, green, and red regions differ in light and heavy chains, because the extent of the deviation vary. Cutoffs are based on visual observation rather than setting a standard value. The cutoffs, in Å, are as follows: light chain: >4.0, blue; between 2.7 and 4.0, green. Deviations <0.5, red; heavy chain: >4.5, blue; between 3.5 and 4.5, green. Deviations <0.5, red. The pictures were generated using molecular graphics package Insight II.

RESULTS

Small RMSDs Between X-Ray Structure and MD Conformers

The system was subjected to equilibration for 10 ps before starting the data collection phase. The conformations at every 20,000 fs time intervals from 1 nsec MD trajectory were analyzed. Each of the 50 MD conformers was superimposed on the X-ray structure of HH63–HEL, and the RMSDs and C_α–C_α deviations were inspected. Light chain and heavy chain were independently inspected. Table 1 shows that overall RMSDs are low, with the values ranging from 1.2 to 2.6 Å.

Largest C_α–C_α Deviations Always Fell in the Same Region: Flexible Regions of the Antibody

Light and heavy chains were inspected for C_α–C_α deviations, and the largest and smallest C_α deviations were noted in each case (Tables 1 and 2). The largest C_α–C_α deviations exhibited by the conformers over the time course of the simulations revealed inherently flexible regions of HH63 binding site (Table 1, Fig. 1). Table 1 also lists the residue positions and the corresponding regions of the largest deviations. The values of the largest deviations are much higher than that of the RMSDs, with the values ranging from 2.7 Å to 15.37 Å for light chain and 3.5 Å to 7.9 Å for heavy chain (*see* Table 1). In the case of the light chain, 45 of 50 conformations show the largest deviations in CDR-2. Importantly, the largest deviations in all of the conformers, except in six, occur in a specific region of CDR-2 of the light chain (*see* Table 1). Of these, in 39 conformations, the largest deviations occur at residue positions $Ser52_L$, $Ser54_L$, $Ile55_L$, $Ser56_L$, or $Gly57_L$, which constitute a turn in CDR-L2 (Fig. 2). Sixteen conformers show the largest deviations at residue position $Ser54_L$, six at position $Ser52_L$, seven at position $Ile55_L$, and six at position $Gly57_L$. Table 3 lists standard deviations at these residue positions. After $Gly57_L$, $Ser54_L$

Table 1
RMSD and C_α Deviations of MD Conformers With Respect to Crystal Structure

HH63–HEL (Time step ps)	RMSD (Å)	Largest deviation (Å)	Corresponding residue and position	Corresponding region
Light chain:				
20	1.231	2.781	Pro 8	*Terminus*
40	1.409	3.126	Ser 52	CDR 2
60	1.466	3.056	Ser 52	CDR 2
80	1.530	3.219	Ser 52	CDR 2
100	1.537	3.239	Ser 52	CDR 2
120	1.568	3.017	Ser 52	CDR 2
140	1.550	2.929	Ser 63	Frame[a]
160	1.624	2.867	Ser 52	CDR 2
180	1.748	3.732	Ser 63	Frame[a]
200	1.834	3.427	Ser 63	Frame[a]
220	1.941	4.216	His 41	Frame
240	1.789	3.481	Ser 63	Frame[a]
260	1.902	4.162	His 41	Frame
280	1.764	4.073	His 41	Frame
300	1.760	3.370	Ser 63	Frame[a]
320	1.865	3.670	His 41	Frame
340	1.783	3.145	Ser 54	CDR 2
360	2.082	5.184	Ser 54	CDR 2
380	1.888	5.550	Ser 54	CDR 2
400	2.053	5.728	Ser 54	CDR 2
420	1.815	5.856	Ser 54	CDR 2
440	1.966	6.168	Ser 54	CDR 2
460	2.180	6.439	Ser 54	CDR 2
480	2.092	6.813	Ser 54	CDR 2
500	2.079	5.800	Ser 54	CDR 2
520	1.978	6.165	Ile 55	CDR 2
540	2.058	5.952	Ser 54	CDR 2
560	2.058	6.162	Ser 54	CDR 2
580	2.088	6.089	Ser 54	CDR 2
600	2.055	6.118	Ser 54	CDR 2
620	2.105	6.626	Ser 54	CDR 2
640	2.216	6.095	Ser 54	CDR 2
660	2.130	5.548	Ser 54	CDR 2
680	2.086	4.580	Ile 55	CDR 2
700	1.997	5.138	Ile 55	CDR 2
720	1.953	4.691	Ile 55	CDR 2
740	2.016	4.738	Ile 55	CDR 2
760	2.198	5.227	Ile 55	CDR 2
780	1.950	5.381	Pro 59	CDR 2
800	2.185	5.857	Ile 55	CDR 2
820	2.245	5.834	Ile 55	CDR 2
840	2.297	9.085	Ser 56	CDR 2
860	2.296	7.530	Pro 59	CDR 2
880	2.219	7.683	Gly 57	CDR 2
900	2.416	12.455	Gly 57	CDR 2
920	2.556	12.923	Ser 56	CDR 2
940	2.360	13.468	Gly 57	CDR 2
960	2.350	13.204	Gly 57	CDR 2
980	2.625	14.485	Gly 57	CDR 2
1000	2.688	15.371	Gly 57	CDR 2

(continues)

Table 1
(continued)

HH63–HEL (Time step ps)	RMSDs (Å)	Largest deviation (Å)	Corresponding residue and position	Corresponding region
Heavy chain				
20	1.231	3.509	Gly 55	CDR 2
40	1.409	4.198	Glu 88	Frame
60	1.466	5.157	Glu 88	Frame
80	1.530	4.240	Glu 88	Frame
100	1.537	5.891	Gly 55	CDR 2
120	1.568	4.224	Asp 27	CDR 1
140	1.550	5.078	Asp 27	CDR 1
160	1.624	5.120	Asp 27	CDR 1
180	1.748	4.359	Asp 27	CDR 1
200	1.834	5.693	Asp 27	CDR 1
220	1.941	5.299	Asp 27	CDR 1
240	1.789	5.347	Asp 27	CDR 1
260	1.902	5.220	Asp 27	CDR 1
280	1.764	5.045	Asp 27	CDR 1
300	1.760	5.025	Asp 27	CDR 1
320	1.865	5.322	Gly 55	CDR 2
340	1.783	4.966	Asp 27	CDR 1
360	2.082	6.696	Asp 27	CDR 1
380	1.888	7.392	Asp 27	CDR 1
400	2.053	7.984	Asp 27	CDR 1
420	1.815	5.633	Asp 27	CDR 1
440	1.966	5.457	Asp 27	CDR 1
460	2.180	5.559	Asp 27	CDR 1
480	2.092	5.230	Asp 27	CDR 1
500	2.079	5.772	Asp 27	CDR 1
520	1.978	5.322	Asp 27	CDR 1
540	2.058	6.623	Asp 27	CDR 1
560	2.058	5.203	Asp 27	CDR 1
580	2.088	6.873	Asp 27	CDR 1
600	2.055	5.694	Asp 27	CDR 1
620	2.105	6.376	Asp 27	CDR 1
640	2.216	6.873	Asp 27	CDR 1
660	2.130	6.520	Asp 27	CDR 1
680	2.086	5.126	Asp 27	CDR 1
700	1.997	6.669	Asp 27	CDR 1
720	1.953	6.414	Asp 27	CDR 1
740	2.016	7.209	Asp 27	CDR 1
760	2.198	6.579	Asp 27	CDR 1
780	1.950	6.133	Asp 27	CDR 1
800	2.185	6.570	Asp 27	CDR 1
820	2.245	6.449	Asp 27	CDR 1
840	2.297	6.869	Asp 27	CDR 1
860	2.296	7.635	Asp 27	CDR 1
880	2.219	7.838	Asp 27	CDR 1
900	2.416	7.330	Asp 27	CDR 1
920	2.556	8.163	Asp 27	CDR 1
940	2.360	6.783	Asp 27	CDR 1
960	2.350	7.242	Asp 27	CDR 1
980	2.625	7.354	Asp 27	CDR 1
1000	2.625	6.986	Asp 27	CDR 1

[a]Region spatially close to CDR-2.

Abbreviations: RMSD = root mean squared deviations; MD = molecular dynamics; HEL = anti-hen egg white lysozyme; CDR = complementarity determining regions.

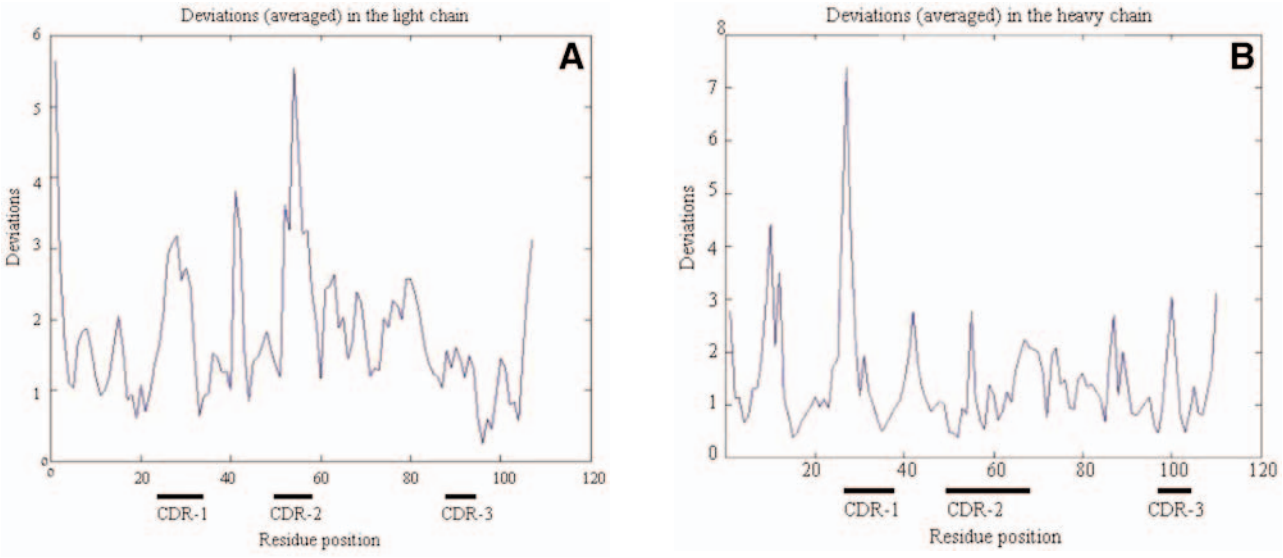

Fig. 1. The deviations in C atom positions of the molecular dynamic conformers with respect to the X-ray crystal structure, in the light chain **(A)** and heavy chain **(B)**. Residue positions are shown on *x*-axis and deviations, in Å, are shown on *y*-axis. Complementarity determining regions (CDRs) are shown with thick horizontal bars.

has a large standard deviation of ±0.826, showing that it undergoes the largest fluctuations (Table 3). The very large standard deviation of ±2.660 at $Gly57_L$ is not surprising owing to the flexible nature of this residue. In five of the remaining six cases the largest deviations fall in regions spatially close to CDR-2 (*see* Table 1). The large deviations occur at similar positions in all conformers and are always in CDR-2 or regions spatially close to CDR-2.

The values of largest deviations in the heavy chain again are quite large, with a range of 3.5–8.1 Å (*see* Table 1). Forty-five of 50 conformations show the largest deviations at the residue position $Asp27_H$. This position is in the coil of CDR-H1, present at the HH63–HEL interface (*see* Fig. 2). The six conformers in which the largest deviations do not fall at $Asp27_H$ position, show the second largest deviations at this position (not shown). Of these, three show the highest deviations in CDR-H2 and another three in the framework region. In the light chain, the largest deviations fall in CDR-2 and are largely exhibited within a linear segment of five residues. In the heavy chain, the largest deviations are exhibited largely by single residue: $Asp27_H$.

Smallest C_α–C_α Deviations Always Fell in the Same Region: Rigid Regions of Antibody

The values of smallest C_α–C_α deviations range from 0.08 to 0.57 Å in light chain and 0.06–0.83 Å in heavy chain (*see* Table 2). In the case of light chain, the lowest or the second lowest deviations in 34 of 50 conformations lie in CDR-L3, whereas 26 of 34 conformations have the smallest deviations in CDR-L3 (*see* Table 2). The smallest deviations at CDR-L3 recur at residue positions $Pro95_L$, $Tyr96_L$, and $Phe98_L$, which constitute a turn. In conformations where the smallest deviations are at the terminus or in frames, the second smallest deviations are exhibited by CDR-L3.

The positions of the smallest deviations in MD conformers are relatively variable in the

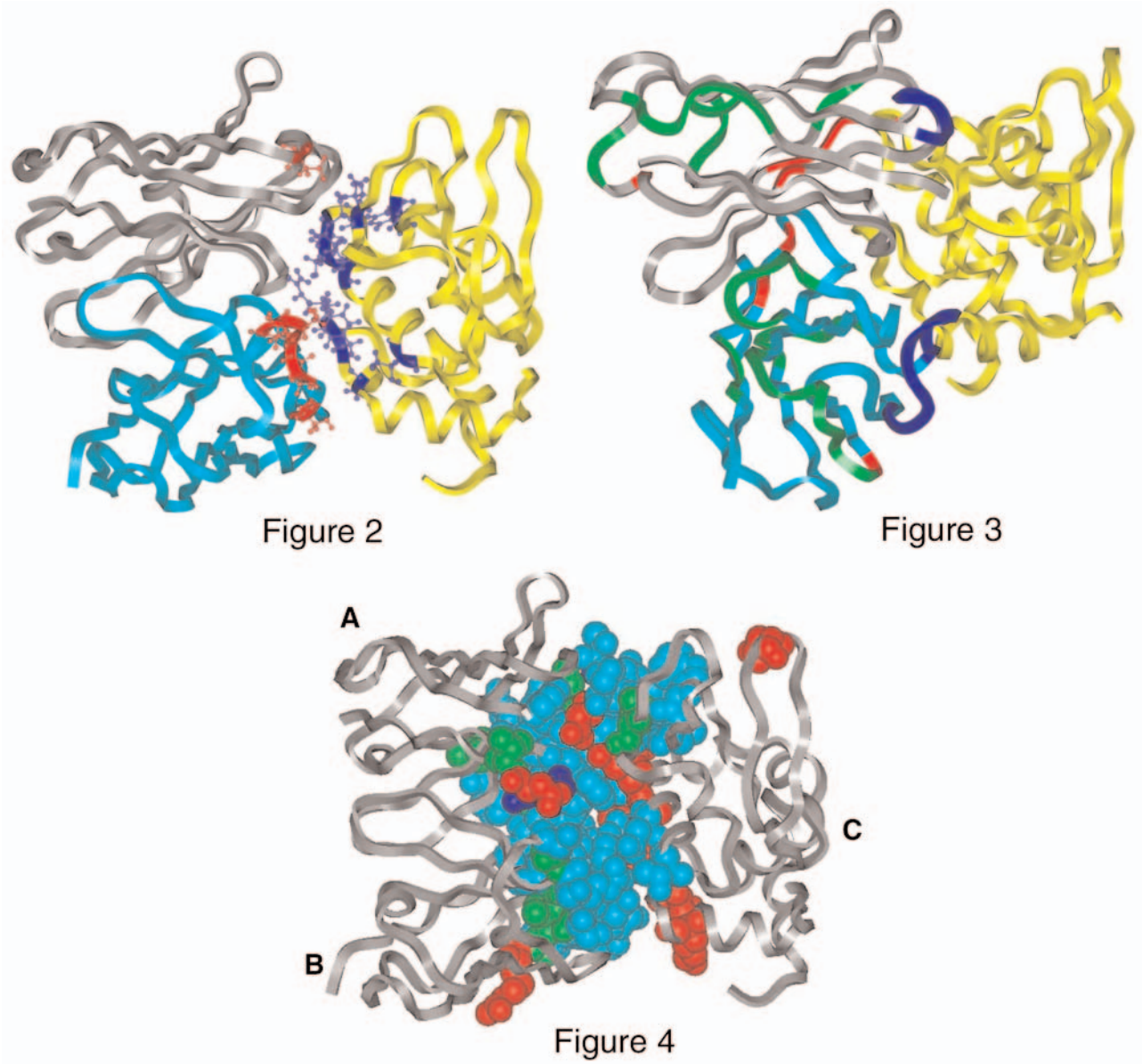

Fig. 2. A ribbon structure of HH63–HEL complex showing the positions of the largest deviating residues. Light chain, heavy chain, and lysozyme are shown in cyan, gray, and yellow, respectively. The largest deviating residues of light and heavy chains are shown in red, with their side chains displayed in ball-and stick-models. Those epitope residues that contribute more than –1.0 kcal/mol toward binding (13,14,30) are shown in purple, with their side chains displayed in ball-and-stick model.

Fig. 3. Flexible and rigid regions of light and heavy chains. Light chain, heavy chain, and lysozyme are shown in cyan, gray and yellow, respectively. The blue color shows the most flexible part, green highlight parts of intermediate flexibility, and red shows the most rigid parts of light and heavy chains. The flexibility assignments are as described in Materials and Methods.

Fig. 4. Residue type at HH63–HEL interface. Interfacial residues are shown in CPK models with their side chains on. Interfacial charged, polar, and hydrophobic residues are shown in red, cyan, and green, respectively. Glycines are shown in dark blue. Chain A, B, and C are heavy chain, light chain, and lysozyme, respectively.

Table 2
Smallest C_α Deviations of MD Conformers With Respect to the Crystal Structure

HH63–HEL (Time step, ps)	Smallest deviation (Å)	Corresponding residue and position	Corresponding region
Light chain			
20	0.196	$Ala25_L$	CDR 1
40	0.238	$Gln27_L$	CDR 1
60	0.121	$Ala25_L$	CDR 1
80	0.230	$Ser26_L$	CDR 1
100	0.108	$Ser43_L$	Frame
120	0.465	$Ser28_L$	CDR 1
140	0.283/0.343	$Ile2_L$/$Tyr96_L$	*terminus*/CDR 3
160	*0.248/0.401*	*$Val3_L$/$Phe98_L$*	*terminus/CDR 3*
180	0.165	$Thr97_L$	*Frame*
200	0.238	$Ala25_L$	CDR 1
220	0.165	$Lys103_L$	Frame[a]
240	0.223	$Lys103_L$	Frame[a]
260	0.088	$Leu104_L$	Frame[a]
280	0.161/0.240	$Asp1_L$/$Gly99_L$	*terminus*/CDR 3
300	0.367	$Leu33_L$	CDR 1
320	0.098	$Pro95_L$	CDR 3
340	0.086	$Phe98_L$	CDR 3
360	0.318	$Pro95_L$	CDR 3
380	0.251	$Tyr96_L$	CDR 3
400	0.322	$Phe98_L$	CDR 3
420	0.208	$Tyr96_L$	CDR 3
440	0.103/0.287	$Ala9_L$/$Pro95_L$	*terminus*/CDR 3
460	0.227	$Pro95_L$	CDR 3
480	0.209	$Tyr96_L$	CDR 3
500	0.420	$Phe98_L$	CDR 3
520	0.313	$Phe98_L$	CDR 3
540	0.366	$Pro95_L$	CDR 3
560	0.133/0.297	$Leu4_L$/$Phe98_L$	*terminus*/CDR 3
580	0.160/0.351	$Thr5_L$/$Pro95_L$	*terminus*/CDR 3
600	0.349	$Ser67_L$	Frame
620	0.218	$Phe98_L$	CDR 3
640	0.329	$Lys103_L$	Frame[a]
660	0.176	$Phe98_L$	CDR 3
680	0.321	$Tyr96_L$	CDR 3
700	0.128	$Thr69_L$	Frame
720	0.520	$Glu79_L$	Frame
740	0.193	$Tyr96_L$	CDR 3
760	0.080	$Tyr96_L$	CDR 3
780	0.124	$Val78_L$	Frame
800	0.179/0.380	$Val3_L$/$Pro95_L$	*terminus*/CDR 3
820	0.292	$Tyr96_L$	CDR 3
840	0.222	$Pro95_L$	CDR 3
860	0.417	$Pro95_L$	CDR 3
880	0.277	$Pro95_L$	CDR 3
900	0.326/0.371	$Asp17_L$/$Pro95_L$	Frame/CDR 3
920	0.574	$Thr10_L$	Frame
940	0.283/0.426	$Ser20_L$/$Tyr96_L$	Frame/CDR 3
960	0.288	$Phe98_L$	CDR 3
980	0.369	$Ser20_L$	Frame
1000	0.310	$Asp70_L$	Frame

(continues)

Table 2
(continued)

HH63–HEL (Time step, ps)	Smallest deviation (Å)	Corresponding residue and position	Corresponding region
Heavy chain			
20	0.155	$Ala96_H$	CDR 3
40	0.067	$Cys22_H$	Frame
60	0.144	$Thr21_H$	Frame
80	0.064	$Trp36_H$	CDR 1
100	0.126	$Trp36_H$	CDR 1
120	0.180	$Trp98_H$	CDR 3
140	0.208	$Tyr94_H$	CDR 3
160	0.284	$Cys95_H$	CDR 3
180	0.242	$Ile69_H$	Frame[b]
200	0.219	$Trp36_H$	CDR 1
220	0.197	$Tyr47_H$	Frame[b]
240	0.160	$Trp34_H$	CDR 1
260	0.220	$Trp34_H$	CDR 1
280	0.298	$Ile37_H$	CDR 1
300	0.223	$Ala96_H$	Frame[c]
320	0.240	$Trp103_H$	CDR 3
340	0.220	$Gln77_H$	Frame
360	0.349	$Thr21_H$	Frame
380	0.383	$Ser52_H$	CDR 2
400	0.231	$Trp36_H$	CDR 1
420	0.229	$Val85_H$	Frame
440	0.288	$Ile51_H$	CDR 2
460	0.066	$Ser97_H$	CDR 3
480	0.348	$Ala96_H$	CDR 3
500	0.221/0.342	$Lys13_H$/$Tyr94_H$	Frame/CDR 3
520	0.217	$Ser84_H$	Frame
540	0.189/0.216	$Thr57_H$/$Ser97_H$	CDR 2/CDR 3
560	0.298	$Tyr79_H$	Frame
580	0.422	$Ile69_H$	Frame[b]
600	0.373	$Ala96_H$	CDR 3
620	0.217	$Tyr78_H$	Frame
640	0.499	$Thr70_H$	Frame
660	0.221	$Ile51_H$	CDR 2
680	0.153	$Ser97_H$	CDR 3
700	0.448	$Tyr50_H$	CDR 2
720	0.159	$Ser35_H$	CDR 1
740	0.177	$Arg71_H$	Frame
760	0.272	$Ala96_H$	CDR 3
780	0.369	$Tyr50_H$	CDR 2
800	0.337	$Arg71_H$	Frame
820	0.473/0.498	$Leu4_H$/$Pro61_H$	Frame/CDR 2
840	0.603	$Ser23_H$	Frame
860	0.254	$Tyr50_H$	CDR 2
880	0.274	$Tyr50_H$	CDR 2
900	0.616	$Tyr50_H$	CDR 2
920	0.601	$Ser35_H$	CDR 1
940	0.271	$Tyr50_H$	CDR 2
960	0.381	$Tyr50_H$	CDR 2
980	0.839	$Leu20_H$	Frame
1000	0.462	$Ser62_H$	CDR 2

[a]Region spatially close to CDR-3.
[b]Region spatially close to CDR-2.
[c]Region spatially close to CDR-3.
See Table 1 for abbreviations.

Table 3
Standard Deviations of Flexible Residues

Position	Standard deviation
Light chain	
$Ser52_L$	±0.139
$Ser63_L$	±0.3363
$His41_L$	±0.2473
$Ser54_L$	±0.8257
$Ile55_L$	±0.6067
$Gly57_L$	±2.6593
Heavy chain	
Gly 55_H	±1.2440
$Glu88_H$	±0.5420
$Asp27_H$	±1.0119

heavy chain (*see* Table 2). However, the smallest deviations most frequently fall in CDR-H3, followed by CDR-H2. In 10 conformations, the lowest deviations are exhibited by $Tyr50_H$ and $Ile51_H$, which are in termini of CDR-H2 (*see* Fig. 2).

Preliminary results on 200 ps–explicit MD simulation of unbound HH63 show that, although the largest deviation for the light chain is still in CDR-2 (residue position: Ser52; Dev- 3.239 Å), for the heavy chain, the largest and second largest deviations fell in frame close to CDR3 and in CDR3 (residue position: Gly100; Dev- 3.087), respectively. The observed flexibility in CDR-H3 in the unbound state is corroborates the finding by Li et al. *(14)* where, based on the superimposition of bound and unbound states, the CDR-H2 and CDR-H3 were suggested to have higher movements.

Assigning Flexible and Rigid Regions of the Antibody: Binding Site Contains Both Flexible and Rigid Regions

We calculated the mean of all C_α deviations of all 50 conformers and plotted them against the residue positions, to inspect the regions of flexibility and rigidity in HH63 (Fig. 3). Regions of largest flexibility lie in the coils of CDRs, followed by the regions of lower flexibility falling in the coils relatively distant from the binding site (*see* Fig. 3). The regions of largest flexibility and largest rigidity both lie at the binding interface, but at different CDRs (*see* Fig. 3). Although all of the variable domains were inspected for C_α–C_α deviations, both the largest and the smallest deviations in almost all the conformations reside at the CDR regions (*see* Fig. 3).

In summary, the largest deviations were always in CDR-L2 and CDR-H1, whereas the smallest deviations were always in CDR-L3 and CDR-H3, and sometimes CDR-H2. This observation indicate that (1) there are inherently locally "flexible" and "rigid" regions of the antibody; (2) both inherent flexible and rigid regions actually are confined to the binding site (CDRs), possibly because of their important roles in molecular recognition; and (3) flexible and rigid regions are exhibited by different CDRs.

Flexible Regions Are Intermolecularly Associated Whereas Rigid Regions Are Not

It has been shown that the binding site undergoes larger fluctuations and involve polar and charged residues where the binding was mainly through the electrostatic contributions of these polar and charged residues *(31)*, and that the charged and polar residues at the flexible region form hydrogen-bond network to complement the shape of binding substrate *(24)*. Nuclear magnetic resonance shows that flexible loops of human tyrosine kinase form the ligand interaction site *(34)*. Figure 4 shows the proportion and distribution of charged and polar residues at HH63 binding site. To determine whether flexible and rigid regions played roles in molecular recognition of a protein antigen by an antibody, we examined the largest and smallest deviating residues for their involvement in intermolecular associations in the HH63-HEL complex. Figure 5 summarizes that both flexible and rigid regions are located at the binding sites.

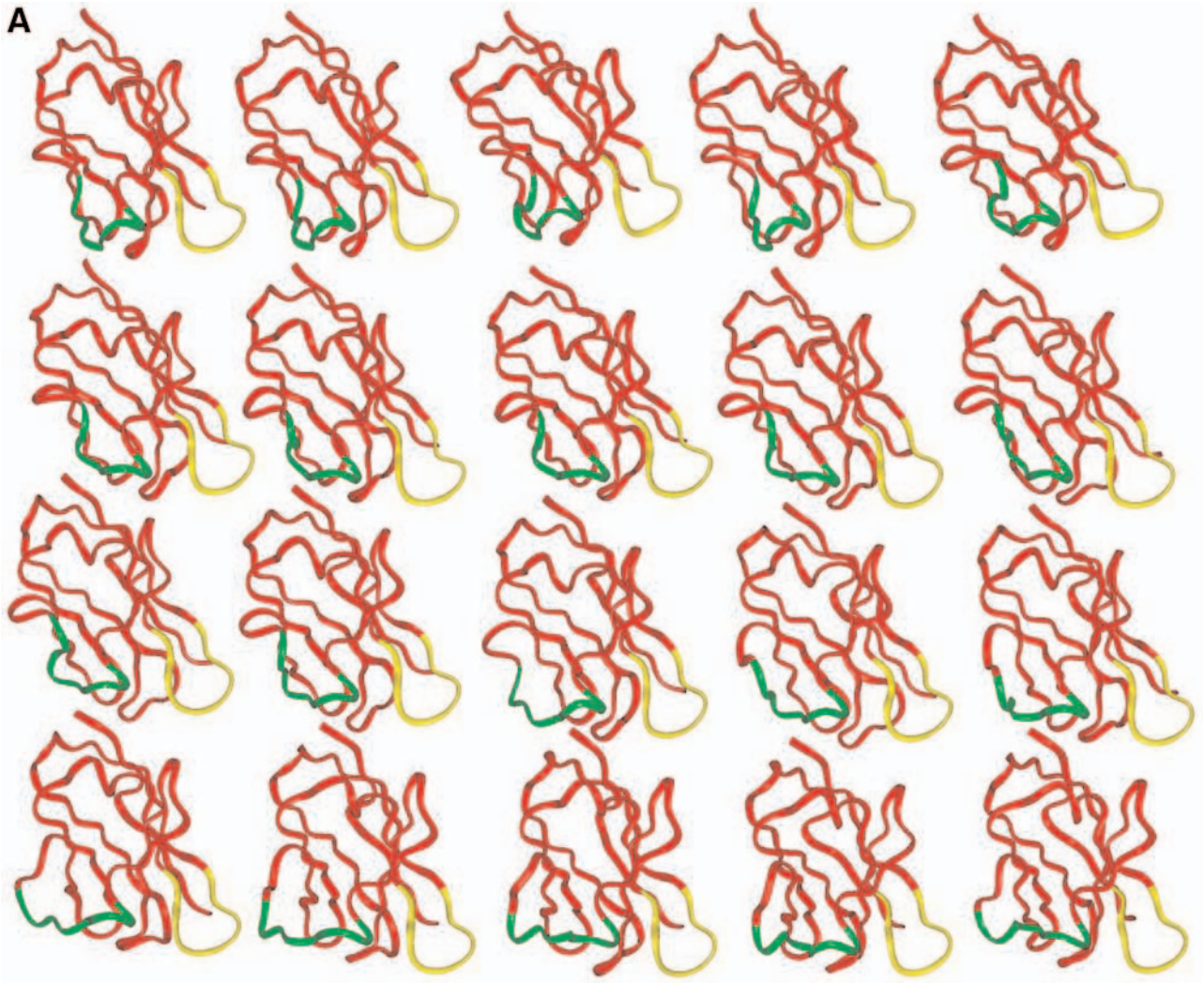

Fig. 5. Conformations of Light-chain **(A)** and Heavy-chain **(B)** extracted from last 200 ps of 1 nsec molecular dynamic trajectory. The conformations shown are extracted at regular time intervals of every 20,000 fs. Complementarity determining region (CDR)-L2 (flexible) is shown in green/dark gray; CDR-L3 (rigid) in yellow/light gray; CDR-H1 (flexible) in red/dark gray; CDR-H3 (rigid) in yellow/light gray. Figure illustrates the fluctuations in flexible CDRs, whereas the conformations of rigid CDRs stay relatively similar. Color is present in the e-Book version exclusively. *(Figure continues)*

The flexible regions of HH63 are located at the binding site and are predominantly composed of polar and charged residues; with the exception of Ile55, the residues showing largest deviations in both the chains are either polar or charged (*see* Table 1). Table 4 lists the intermolecular associations of largest and smallest deviating residues. The residues were considered to be intermolecularly associated when the distance between their C_α atoms were ≤12 Å to qualitatively access the involvement of flexible regions in intermolecular associations compared with rigid regions. In the crystal structure (Table 4) and for 100 MD conformers extracted during 800–1000 ps (*see* Table 4), larger deviating residues show higher inter-chain and intermolecular associations (Fig. 6), whereas small deviating residues do not have

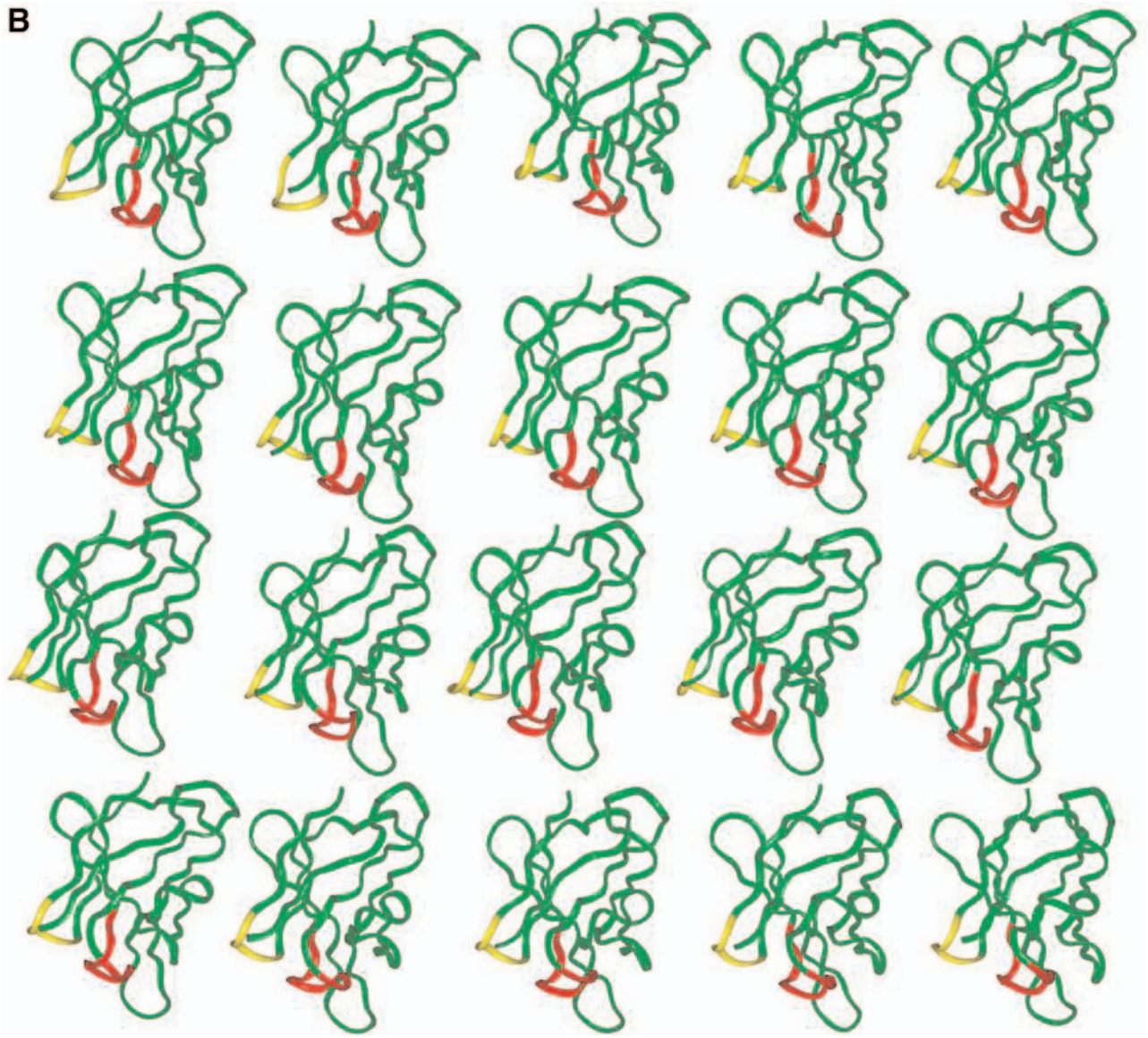

Fig. 5. *(continued)*

close associations with HEL (Fig. 7). CDR-L3 and CDR-H3 are rigid regions and are not as close to HEL in the X-ray crystal structure, whereas CDR-L2 and CDR-H1, constituting flexible regions, are close to HEL in the X-ray crystal structure. With the exception of $Gly57_L$, all large deviating residues have intermolecular interactions. $Asp27_H$ shows the largest deviations in all the analyzed conformers and has close associations with five HEL residues. Furthermore, larger deviating residue shows additional associations during the MD simulation (*see* Table 4, Fig. 6). $Ser54_L$ has close associations with eight HEL residues during the MD simulation. With the exception of $Gly57_L$, all the large deviating residues, $Ser52_L$, $Ser54_L$, $Ile55_L$, and $Asp27_H$ not only have intermolecular associations with HEL, but also are in close association with many different HEL residues (*see* Table 4). Associations with

Table 4
Intermolecular and Interchain Interactions

Residue	Interaction	C_α–C_α distance[a] (Å)	Interchain[b]	Intermolecular crystal structure	MD conformers[c]
Residues with large deviations					
$Ser52_L$	$Ser52_L$-$Thr89_Y$	11.190		√	√
	$Ser52_L$-$Asp87_Y$				√
	$Ser52_L$-$Ile88_Y$				√
	$Ser52_L$-$Ala90_Y$				√
	$Ser52_L$-$Val92_Y$				√
	$Ser52_L$-$Asn93_Y$				√
$Ser54_L$	$Ser54_L$-$Thr89_Y$	11.542		√	√
	$Ser54_L$-$Asp87_Y$				√
	$Ser54_L$-$Ala90_Y$				√
	$Ser54_L$-$Asn93_Y$				√
	$Ser54_L$-$Ser85_Y$				√
	$Ser54_L$-$Ser86_Y$				√
	$Ser54_L$-$Ile88_Y$				√
	$Ser54_L$-$Val92_Y$				√
$Ile55_L$	$Ile55_L$-$Gly99_H$	11.288	√		
	$Ile55_L$-$Gly100_H$	10.955	√		
	$Ile55_L$-$Asp101_H$	8.992	√		
	$Ile55_L$-$Asp101_H$	8.976	√		
	$Ile55_L$-$Thr89_Y$				√
	$Ile55_L$-$Ala90_Y$				√
	$Ile55_L$-$Asp87_Y$				√
	$Ile55_L$-$Ile88_Y$				√
$Gly57_L$	$Gly57_L$-$Asp101_H$	10.777	√		
	$Gly57_L$-$Asp101_H$	10.756	√		
$Asp27_H$	$Asp27_H$-$Ser72_Y$	11.687		√	√
	$Asp27_H$-$Arg73_Y$	9.197		√	√
	$Asp27_H$-$Asn74_Y$	10.247		√	√
	$Asp27_H$-$Leu75_Y$	10.553		√	√
	$Asp27_H$-$Asn77_Y$	10.782		√	
	$Asp27_H$-$Gly71_Y$				√
	$Asp27_H$-$Trp62_Y$				√
	$Asp27_H$-$Thr69_Y$				√
	$Asp27_H$-$Pro70_Y$				√
Residues with small deviations					
$Phe98_L$	None				
$Pro95_L$	$Pro95_L$-$Ser100_Y$	11.828		√	√
$Tyr96_L$	$Tyr96_L$-$Trp98_H$	10.884	√		
	$Tyr96_L$-$Ser100_Y$				√
$Ala96_H$	None				

[a]Intermolecular distances are shown only of the crytal structure.
[b]Interchain interactions are only shown for the crystal structure.
[a,c]Interactions shown for MD conformers are those found during 800–1000 ps time stage. Their distances and distribution in 100 conformers are depicted in Fig. 4.
See Table 1 for abbreviations.

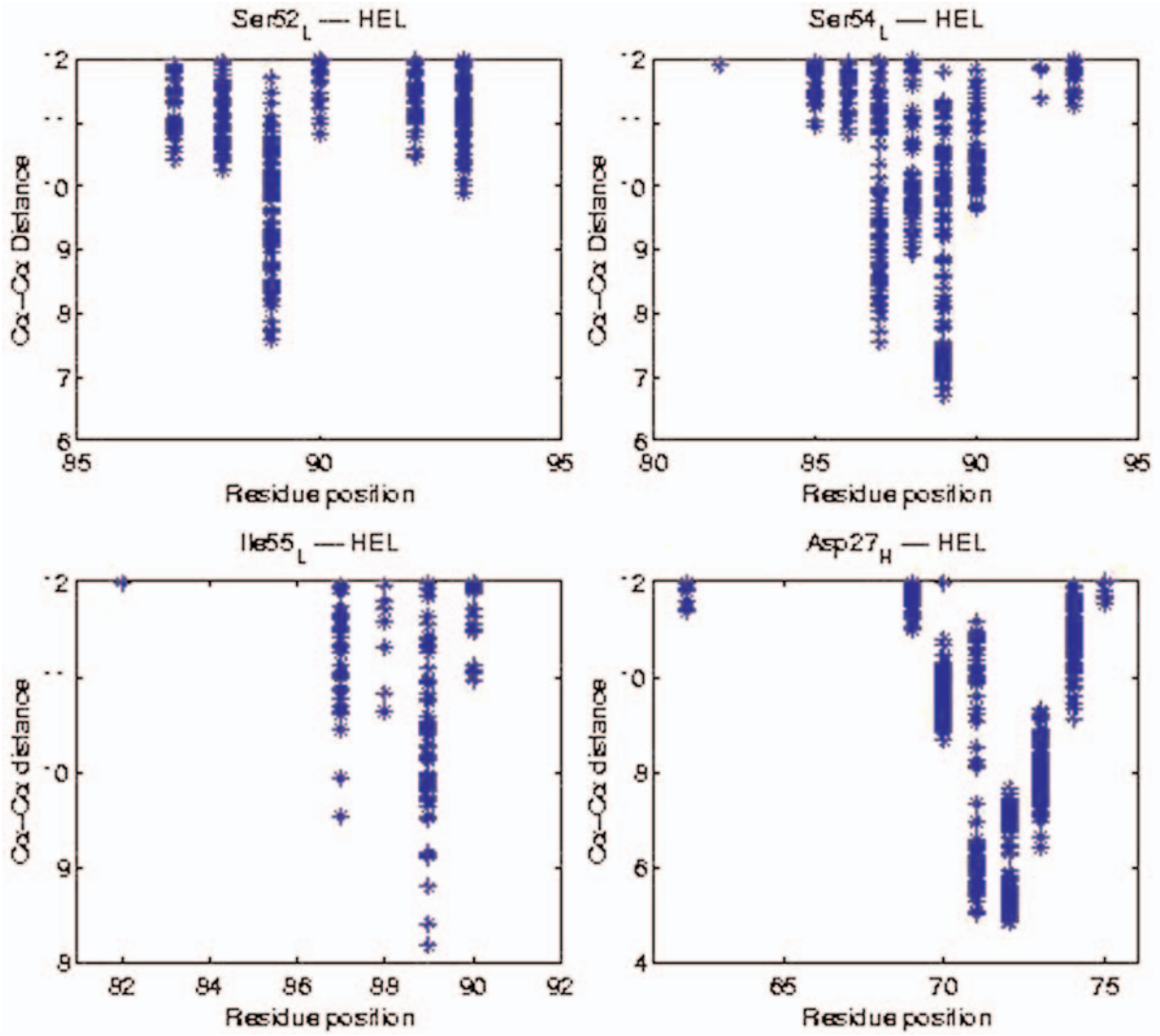

Fig. 6. Intermolecular interactions of the most deviating residues of light and heavy chains. Intermolecular interactions are shown for 100 conformations during 800–1000 ps time of the molecular dynamic simulation.

different HEL residues are seen in $Asp27_H$ in crystal structure and in $Ser52_L$, $Ser54_L$, and $Ile55_L$ during the MD simulation. These associations during the MD simulation are seen in large number of MD conformers (*see* Fig. 6), suggesting a functional importance of these associations.

In contrast, residues that deviate least in both heavy and light chain do not form close associations with HEL (*see* Table 4). None of the close-range associations with HEL were detected for $Phe98_L$ and $Ala96_H$ in either crystal structure or in any of the conformations extracted from the MD simulation during 800–1000 ps (*see* Table 4). $Pro95_L$ has one intermolecular association with $Ser100_Y$ in both crystal structure and MD conformers (*see* Fig. 7). $Tyr96_L$ also is in close association with $Ser100_Y$ in MD conformers (*see* Fig. 7). The intermolecular associations of $Pro95_L$ and $Tyr96_L$

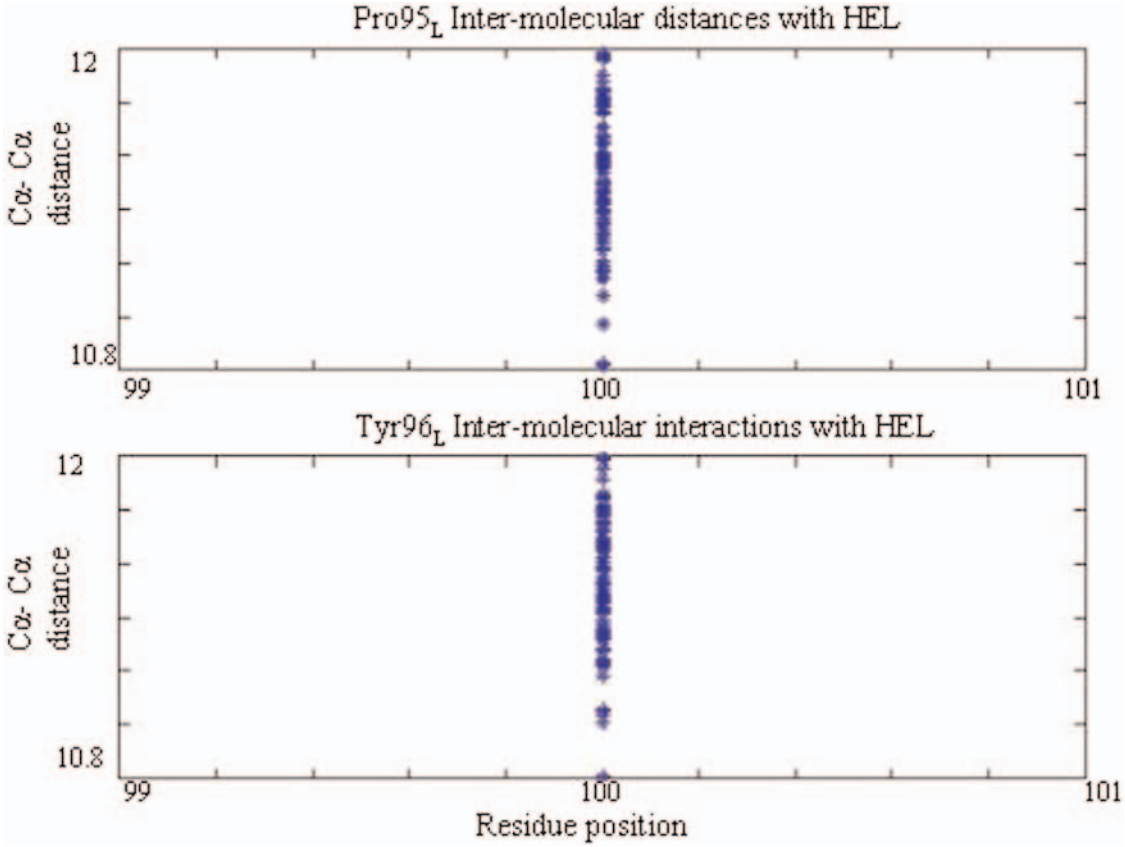

Fig. 7. Intermolecular interaction of $Pro95_L$ and $Tyr96_L$. Intermolecular interactions are shown for 100 conformations during 800–1000 ps time of the molecular dynamic simulation.

occur in large number of MD conformers (*see* Fig. 7). It should be noted that these two residues are in close association with only one epitope residue, in contrast to large deviating residues, which are in close association to many different HEL residues (*see* Table 4, Fig. 6).

In summary, larger deviating residues form greater numbers of intermolecular associations with multiple residues, whereas least deviating residues, or rigid parts, do not form intermolecular associations, and are generally away from HEL. Our results show that flexible parts (1) are mostly constituted by polar or charged residue, at least in this case, and (2) the functional role of flexible residues are to form intermolecular associations. CDR-H1 is the most flexible in heavy chain and is the only CDR involved in an intermolecular salt bridge, connecting $Asp32_H$ to $Lys97_Y$ *(1,13,30)*. $Lys97_Y$ is a "hot spot" epitope residue in HH63–HEL complex and in three other HEL complexes of antibodies belonging to the same family *(12,30,35,29)*. This intermolecular interaction in these complexes have been shown to be significantly important for binding, both computationally *(26)* and experimentally *(35, 30)*. Furthermore, light chain forms larger intermolecular interactions, and thus it is likely that flexible and rigid regions are more rigorously selected in light chain than in heavy. This is further corroborated by the observation that in light chain, the flexible regions are same in bound and upbound form. Flexible regions here are selected *a priori* for

intermolecular interactions, whereas in the heavy chain, the flexible regions in the CDRs of bound and unbound forms are different.

Partly flexible and partly rigid binding seems to be evolutionary selected for optimized binding. The optimized binding is as reflected by experimentally shown high affinity *(13)*, high specificity (Sinha et al., unpublished results) and electrostatic complementarity between HH63 and HEL *(1)*.

DISCUSSION

Our observations show that (1) antibody binding site contains inherent flexible and rigid regions; (2) the regions of flexibility and rigidity lie at the binding interface for their respective roles in binding; (3) flexible parts, made up of polar and charged residues are involved in more intermolecular interactions compared with rigid parts; and (4) formation of this large protein–protein complexes involves partly induced fit and partly lock-and-key type of binding. The residues of smaller deviations may not have clearly defined structural and functional significance or they more likely provide a functional frame work for more flexible parts. The flexible regions form hydrogen bonds and salt bridges on association. This observation is consistent with findings in other proteins. For example, the binding cavity of T4 lysozyme contains two parts—flexible and rigid regions *(23,36)*. The flexibility between domains of tyrosine phosphatase α is proposed to play important roles in establishing functionally important intermolecular and intramolecular interactions *(37)*. The active site of aminotransferase consists of flexible and rigid regions, whereas flexible side chains of polar and charged residues (Asp, Lys, Asn, Arg, and Ser) played important roles in binding *(24)*. Importantly, both the regions of largest flexibility and the regions of least flexibility reside at the binding interface, but at different locations. The regions of intermediate flexibility, which may provide hinge points *(38)* of conformational adjustments on binding, reside in coils away from the binding interface (*see* Fig. 3).

Unlike protein ligand interactions, where the binding interface is of the order of 80–100 $Å^2$ *(39)* and the ligand may fit into a "preconfigured" cavity or grove, protein binding may bury up to a 2200 $Å^2$ area. Anti-HEL antibodies bury 1200–1400 $Å^2$ of area on complex formation. Thus the binding sites of a large protein–protein complex, such as antibody-protein complex, are best described as a mosaic of preconfigured and flexible regions. The flexible regions, undergoing localized induced fit, are destined for intermolecular associations, whereas rigid regions, conforming to lock-and-key mode of binding, provide structural framework.

The flexible regions in light and heavy chains of HyHEL63 are always in CDR-2 and CDR-1, respectively. The rigid regions reside in CDR-3 in case of the light chain. However, in the heavy chain, the rigid regions are in CDR-2 in some conformers and in CDR-3 in others. In a significant number of conformations, the least deviating regions reside in CDR-1 or in frame. It may also be possible that the rigid regions are not rigorously selected in the heavy chain during the affinity maturation of this antibody. The flexible regions associate with HEL, whereas rigid regions do not directly interact with HEL.

The functional importance of protein flexibility is now widely realized *(15,17,40–42)*. Proteins undergo large- and small-scale movements to perform their function *(38,43)*. Protein folding, binding, function, or catalysis all involve flexibilities to varying extents. Thus flexibilities are preselected in the primary sequences. MD approaches has been widely used to study protein internal motions and dynamics required by structure to perform function *(44–49)*. Structural comparisons between mutant and wild-type proteins and MD simulations have shown that protein flexible regions are important for function *(22,16)*. Thus flexible and rigid parts are predefined in the protein structure and are selected for function. The important role of protein flexibilities in protein binding and function has been addressed *(1,17–20)*. The inherent flexible regions at HH63 binding site

are likely a prerequisite for a high-affinity binding. The effects from changes in the environment *(50)*, mutations *(16)*, or binding *(10,51)* are propagated through the flexible parts of the proteins. Thus the present observation of the selective enrichment of conformational substates would be consistent to the previous observation *(16)*, meaning that conformational substates are nonuniformally distributed. Thus flexible and rigid regions are not just an outcome of packing defects or structural details; rather, they are selected during protein evolution for optimized folding, binding, and function.

HyHEL63 observe significantly high affinity toward HEL (*13*). We propose that the binding site of a high-affinity antibody contains flexible and rigid regions, which have functional significance. Such flexible and rigid regions can also be present in germline antibodies. Our work illustrates a direct structure-function relationship in a high-affinity antibody-antigen interactions. This study provides an insight on the mechanism of molecular recognition of a protein antigen by the antibody. The structural and thermodynamic importance of largest and smallest deviating residues can be further verified experimentally. Importantly, there was no correlation between detected flexible regions and crystallographic B-factors, corroborating that these flexible regions are evolutionally selected. B-factors can be an artifact. Earlier studies have shown that the flexible regions important for function do not necessarily fall in the regions of highest B-factors values (*16*). This approach can also be used to pinpoint hot spots of intermolecular associations. Studies are in progress to identify such regions, which are likely also present at the HEL binding site.

CONCLUSIONS

Proteins are made up of flexible and rigid regions. Flexible regions are selected to perform function *(16,17)*. Short-range electrostatic interactions are usually avoided in the flexible parts of the protein, allowing hinge-bending transitions *(17,18,26)*. The present study highlights that affinity maturation of a secondary antibody involves the selection of flexible parts containing polar and charged residues destined for molecular associations during immune responses. Here we have shown inherent flexible and rigid regions of the binding site of the antibody HH63. We conclude that flexible regions, made up of polar and charged residues, are the sites of molecular specificity. Figure 4 illustrates a high proportion of polar and charged residues at the binding interface. We suggest that for molecular recognition or during the affinity maturation, the flexible regions are selected with polar and charged residues so that they first form the encounter complex, involving small conformational adjustments, and then form docked complex via salt bridges, hydrogen bonds, and Van der-Waals contacts. We propose that binding affinity and specificity is mediated through mosaic of flexible and rigid regions. Flexible regions undergo localized induced fit and form intermolecular associations (at least in this complex), whereas rigid regions maintain preconfigured configuration and function primarily as supporting framework. It has been suggested that antibody affinity maturation involves a reduction of conformational flexibility through formation of preconfigured binding site specified by intramolecular polar interactions. We suggest the binding site evolves to a architecture supporting a mosaic of flexible and rigid regions. Flexible regions undergo localized induced fit to optimize interactions with a specified antigen.

ACKNOWLEDGMENTS

We thank Claudia A. Lipschultz and Suja Joseph for helpful discussions. Advanced Biomedical Computing Center personnel are thanked for computational resources and related assistance. The personnel at NCI-Frederick are thanked for their assistance.

REFERENCES

1. Sinha, N. and Smith-Gill, S. J. (2002) Electrostatics in protein binding and function. *Curr. Prot. Pept. Sci.* **3,** 601–614.
2. Kabat, E. A., Wu, T. T., and Bilofsky, H. (1977) Unusual distributions of amino acids in complementarity-determining (hyper-variable) segments of heavy and light chains of immunoglobulins and their possible roles in specificity of antibody-combining sites. *J. Biol. Chem.* **252,** 6609–6616.
3. Dall'Acqua, W., Goldman, E. R., Lin, W., Teng, C., Tsuchiya, D., Li, H., et al. (1998) A mutational analysis of binding interactions in an antigen-antibody protein–protein complex. *Biochemistry* **37,** 7981–7991.
4. Wilson, I. A. and Stanfield, R. L. (1993) Antibody-antigen interactions. *Curr. Opin. Struc. Biol.* **3,** 113–118.
5. Braden, B. C. and Poljak, R. J. (1995) Structural features of the reactions between antibodies and protein antigens. *FASEB J.* **9,** 9–16.
6. Smith-Gill, S. J. (1991) Protein–protein interactions: structural motifs and molecular recognition. *Curr. Opin. Biotech.* **2,** 568–575.
7. Tsumoto, K., Ueda, Y., Maenaka, K., Watanabe, K., Ogasahara, K., Yutani, K., et al. (1994) Contribution to antibody-antigen interaction of structurally perturbed antigenic residues upon antibody binding. *J. Biol. Chem.* **269,** 28777–28782.
8. Chong, L. T., Duan, Y., Wang, L., Massova, I., and Kollman, P. A. (1999) Molecular dynamics and free energy calculations applied to affinity maturation in antibody 48G7. *Proc. Natl. Acad. Sci. USA* **96,** 14330–14335.
9. Novotny, J., Bruccoleri, R. E., and Saul, F. A. (1989) On the attribution of binding energy in antigen-antibody complexes McPC 603, D1.3, and HyHEL5. *Biochemistry* **28,** 4735–4749.
10. Freire, E. (1999)The propagation of binding interactions to remote sites in proteins: Analysis of the binding of the monoclonal antibody D1.3 to lysozyme. *Proc. Natl. Acad. Sci. USA* **96,** 10118–10122.
11. Sundberg, E. J., Urrutia, M., Braden, B. C., Isern, J., Tsuchiya, D., Fields, B. A., et al. (2000) Estimation of the hydrophobic effect in an antigen-antibody protein–protein interface. *Biochemistry* **39,** 15375–15387.
12. Wibbenmeyer, J. A., Schuck, P., Smith-Gill, S. J., and Willson, R. C. (1999) Salt-links dominate affinity of antibody HyHEL-5 for lysozyme through enthalpic contributions. *J. Biol. Chem.* **274,** 26838–26842.
13. Li, Y., Li, H., Smith-Gill, S. J., and Mariuzza, R. A. (2000) Three-dimensional structures of the free and antigen-bound Fab from monoclonal antilysozyme antibody HyHEL-63. *Biochemistry* **39,** 6296–6309.
14. Li, Y., Lipschultz, C. A., Mohan, S., and Smith-Gill, S. J. (2001) Mutations of an epitope hot-spot residue alter rate limiting steps of antigen-antibody protein–protein associations. *Biochemistry* **40,** 2011–2022.
15. Sundberg, E. J. and Mariuzza, R. A. (2000) Luxury accommodations: the expanding role of structural plasticity in protein–protein interactions. *Structure Fold Des.* **8,** R137–R142.
16. Sinha, N. and Nussinov, R. (2001) Point mutations and sequence variability in proteins: redistributions of preexisting populations. *Proc. Natl. Acad. Sci. U. S. A.* **98,** 3139–3144.
17. Sinha, N., Kumar, S., and Nussinov, R. (2001) Interdomain interactions in hinge-bending transitions. *Structure Fold Des.* **9,** 1165–1181.
18. Sinha, N., Tsai, C. J., and Nussinov, R. (2001) Building blocks, hinge-bending motions and protein topology. *J. Biomolec. Struct. Dyn.* **19,** 369–380.
19. Sinha, N. and Smith-Gill, S. J. (2002) Protein structure to function via dynamics. *Protein Pept. Lett.* **9**, 367–377.
20. Carlson, H. A. (2002) Protein flexibility and drug design: how to hit a moving target. *Curr. Opin. Chem. Biol.* **6,** 447–452.
21. Carlson, H. A. (2002) Protein flexibility is an important component of structure-based drug discovery. *Curr. Pharm. Des.* **8,** 1571–1578.
22. Zoete, V., Michielin, O., and Karplus, M. (2002) Relation between sequence and structure of HIV-1 protease inhibitor complexes: a model system for the analysis of protein flexibility. *J. Mol. Biol.* **315,** 21–52.
23. Morton, A. and Matthews, B. W. (1995) Specificity of ligand binding in a buried nonpolar cavity of T4 lysozyme: linkage of dynamics and structural plasticity. *Biochemistry* **34,** 8576–8588.
24. Okamoto, A., Ishii, S., Hirotsu, K., and Kagamiyama, H. (1999) The active site of Paracoccus denitrificans aromatic amino acid aminotransferase has contrary properties: flexibility and rigidity. *Biochemistry* **38,** 1176–1184.
25. Jimenez, R., Salazar, G., Baldridge, K. K., and Romesberg, F. E. (2003) Flexibility and molecular

recognition in the immune system. *Proc. Natl. Acad. Sci. USA* **100**, 92–97.
26. Sinha, N., Mohan, S., Lipschultz, C. A., and Smith-Gill, S. J. (2002) Differences in electrostatic properties at antibody-antigen binding sites: implications for specificity and cross-reactivity. *Biophys. J.* **83,** 2946–2968.
27. Mohan, S., Sinha, N., and Smith-Gill, S. J. (2003) Modeling the binding sites of anti-hen egg white lysozyme antibodies HyHEL-8 and HyHEL-26: an insight into the molecular basis of antibody cross-reactivity and specificity. *Biophys. J*. **85,** 3221–3236.
28. Wedemayer, G. J., Patten, P. A., Wang, L. H., Schultz, P. G., and Stevens, R. C. (1997) Structural insights into the evolution of an antibody combining site. *Science* **276,** 1665–1669.
29. Betts, M. J. and Sternberg, M. J. (1999) An analysis of conformational changes on protein–protein association: implications for predictive docking. *Protein Eng.* **12,** 271–283.
30. Li, Y., Urrutia, M., Smith-Gill, S. J., and Mariuzza, R. A. (2003) Dissection of binding interactions in the complex between the anti-lysozyme antibody HyHEL-63 and its antigen. *Biochemistry* **42,** 11–22.
31. Peters, G. H., Frimurer, T. M., Andersen, J. N., and Olsen, O. H. (2000) Molecular dynamics simulations of protein-tyrosine phosphatase 1B. II. substrate-enzyme interactions and dynamics. *Biophys J.* **78,** 2191–2200.
32. Maple, J. R., Dinur, U., and Hagler, A. T. (1988) Derivation of force fields for molecular mechanics and dynamics from ab initio energy surfaces. *Proc. Natl. Acad. Sci. USA* **85,** 5350–5354.
33. Bernstein, F., Koetzle, T., Williams, G., Meyer, E. J., Brice, M., Rodgers, J.,et al. (1997) The protein data bank: a computer based archival file for macromolecular structures. *J. Mol. Biol.* **112,** 535–542.
34. Hiroaki, H., Klaus, W., and Senn, H. (1996) Determination of the solution structure of the SH3 domain of human p56 Lck tyrosine kinase *J. Biomolec. N. M. R.* **8,** 105–122.
35. Pons, J., Rajpal, A., and Kirsch, J. F. (1999) Energetic analysis of an antigen/antibody interface: alanine scanning mutagenesis and double mutant cycles on the HyHEL-10/ lysozyme interaction. *Protein Sci.* **8,** 958–968.
36. Morton, A., Baase, W. A., and Matthews, B. W. (1995) Energetic origins of specificity of ligand binding in an interior nonpolar cavity of T4 lysozyme. *Biochemistry* **34,** 8564–8575.
37. Sonnenburg, E. D., Bilwes, A., Hunter, T., and Noel, J. P. (2003) The structure of the membrane distal phosphatase domain of RPTPa reveals interdomain flexibility and an SH2 domain interaction region. *Biochemistry* **42,** 7904–7914.
38. Gerstein, M. and Krebs, W. (1998) A database of macromolecular motions. *Nucleic Acids Res.* **26,** 4280–4290.
39. Luque, I. and Freire, E. (2000) Structural stability of binding sites: consequences for binding affinity and allosteric effects. *Proteins Struct. Func. Genet.* **4,** 63–71.
40. Tsou, C. L. (1993) Conformational flexibility of enzyme active sites. *Science* **262,** 380–381.
41. Wilson, M. A. and Brunger, A. T. (2000) The 1.0 A crystal structure of Ca(2+)-bound calmodulin: an analysis of disorder and implications for functionally relevant plasticity. *J. Mol. Biol.* **301,** 1237–1256.
42. Trikha, J., Theil, E. C., and Allewell, N. M. (1995) High resolution crystal structures of amphibian red-cell L ferritin: potential roles for structural plasticity and solvation in function. *J. Mol. Biol.* **248,** 949–967.
43. Gerstein, M., Schulz ,G., and Chothia, C. (1993) Domain closure in adenylate kinase. Joints on either side of two helices close like neighboring fingers. *J. Mol. Biol.* **229,** 494–501.
44. Karplus, M. and McCammon, J. A. (2002) Molecular dynamics simulations of biomolecules. *Nat. Struct. Biol.* **9,** 646–652.
45. McCammon, J. A. and Harvey, S. (1987) *Dynamics of Proteins and Nucleic Acids.* Cambridge University Press, Cambridge, UK.
46. Brooks, C. L. III., Karplus, M., and Pettitt, B. M. (1988) *Proteins: A Theoretical Perspective of Dynamics, Structure and Thermodynamics.* John Wiley and Sons, New York.
47. J. Ma, P. B. Sigler, Z. Xu and M. Karplus, A dynamic model for the allosteric mechanism of GroEL. *J. Mol. Biol.* **302,** 303–313 (2000).
48. Young, M. A., Gonfloni, S., Superti-Furga, G., Roux, B., and Kuriyan, J. (2001) Dynamic coupling between the SH2 and SH3 domains of c-Src and Hck underlies their inactivation by C-terminal tyrosine phosphorylation. *Cell* **105,** 115–126.
49. Yang, C., Jas, G. S., and Kuczera, K. (2004) Structure, dynamics and interaction with kinase

targets: computer simulations of calmodulin. *Biochim. Biophys. Acta* **1697,** 289–300.
50. Kumar, S., Ma, B., Tsai, C. J., Sinha, N., and Nussinov, R. (2000) Folding and binding cascades: dynamic landscapes and population shifts. *Protein Sci.* **9,** 10–9.
51. Tsai, C. J., Ma, B., and Nussinov, R. (1999) Folding and binding cascades: shifts in energy landscapes. *Proc. Natl. Acad. Sci. USA* **96,** 9970–9972.